Check for updates

Polymer Composites

WILEY | spe INSPIRING PLASTICS PROFESSIONALS

RESEARCH ARTICLE OPEN ACCESS

Multifunctional Epoxy Composites Reinforced With Hybrid MWCNT/Graphene-Related Materials Buckypaper

Thais Ferreira da Silva[1,2] | Thiély Ferreira da Silva[3] | Rieyssa Maria de Almeida Corrêa[3] | Rui Alexandre Araújo Ribeiro[2] | Braian Esneider Buitrago Uribe[2] | Michelle Leali Costa[1,4] | Delfim Fernandes Soares[2] | Fabio Roberto Passador[3] | Beate Krause[5] | Maria Conceição Paiva[2] | Edson Cocchieri Botelho[1]

[1]Faculty of Engineering, São Paulo State University (UNESP), Guaratinguetá, Brazil | [2]School of Engineering, University of Minho, Guimarães, Portugal | [3]Department of Science and Technology, Polymer and Biopolymer Technology Laboratory (TecPBio), Federal University of São Paulo (UNIFESP), São José dos Campos, Brazil | [4]Ganesha Institute of Innovation Science and Technology, São José dos Campos, Brazil | [5]Instituto Leibniz de Pesquisa de Polímeros Dresden Química Macromolecular, Dresden, Germany

Correspondence: Thais Ferreira da Silva (thais.ferret@hotmail.com)

Received: 2 July 2026 | **Revised:** 24 July 2026 | **Accepted:** 27 July 2026

Keywords: buckypaper | carbon nanotubes | epoxy resin | graphene | structural composites

ABSTRACT

This study investigates the development of multifunctional epoxy composites reinforced with hybrid buckypapers composed of multi-walled carbon nanotubes (MWCNTs) and graphene-related materials (GRMs), including nanographite (NG) and graphene nanoplatelets (GNP). Hybrid buckypapers with different MWCNT/GRM ratios (25/75, 50/50, and 75/25 wt%) were processed via vacuum filtration and subsequently integrated into epoxy matrices through vacuum infusion. The results demonstrate that the architecture and composition of the hybrid buckypapers strongly govern the electrical, thermal, viscoelastic, and electromagnetic performance of the resulting composites. A synergistic interaction between one-dimensional MWCNTs and two-dimensional GNP promoted the formation of interconnected conductive pathways, enhancing charge transport and electromagnetic attenuation. The formulation containing 25 wt% MWCNT and 75 wt% GNP exhibited the best multifunctional performance, achieving electrical conductivity in the order of 10^{-5} S m^{-1} and electromagnetic shielding effectiveness up to 40 dB. Thermogravimetric analysis (TGA) revealed increased thermal stability and carbon residue, while dynamic mechanical analysis (DMA) showed that the viscoelastic response depends on the balance between nanocarbon network continuity and resin infiltration. Microstructural observations confirmed efficient resin impregnation and strong interfacial interactions, which directly influenced the multifunctional response. Overall, the results demonstrate that hybrid MWCNT/GRM buckypapers act as tunable interlayers with multiple functionalities, enabling controlled optimization of electrical conductivity, electromagnetic shielding, and mechanical performance in epoxy composites, with strong potential for lightweight structural and electromagnetic management applications.

1 | Introduction

Advances in the development of composite materials have played a fundamental role in enabling lighter, stronger, and increasingly multifunctional solutions, particularly in the aeronautics, automotive, electronics, and renewable energy sectors [1–3]. In this context, carbon nanomaterials, such as carbon nanotubes (CNTs) and GNP, stand out for their unique combination of mechanical, electrical, and thermal properties [4–6]. Among polymer matrices, epoxy resins are widely used due to their excellent mechanical strength, chemical resistance, dimensional stability, and strong adhesion to various reinforcements. These thermosetting polymers provide an ideal platform for integrating nanocarbon reinforcements, offering a balance between processability and performance. However, despite their high intrinsic stiffness and versatility, epoxy systems are electrically insulating, and although their mechanical behavior

This is an open access article under the terms of the Creative Commons Attribution License, which permits use, distribution and reproduction in any medium, provided the original work is properly cited.

© 2026 The Author(s). *Polymer Composites* published by Wiley Periodicals LLC on behalf of Society of Plastics Engineers.

Highlights

- Hybrid MWCNT/GRM buckypapers were produced by vacuum filtration.
- Buckypaper architecture governed multifunctional composite performance.
- MWCNT/GNP synergy enhanced electrical and EMI shielding properties.
- Epoxy composites achieved EMI shielding effectiveness up to 40 dB.
- Resin infiltration controlled the balance between conductivity and stiffness.

can range from flexible to brittle, highly crosslinked formulations commonly exhibit brittle characteristics [7–9]. Therefore, the incorporation of CNTs and GNPs can impart multifunctionality by improving toughness, electrical conductivity, and thermal stability; nevertheless, achieving uniform dispersion and efficient load transfer remains a significant challenge. The strong tendency of CNTs and GNPs to agglomerate hampers both dispersion and load transfer, resulting in properties that are inferior to those theoretically predicted [10, 11]. Therefore, several processing strategies have been developed to overcome these limitations and enable the production of high-performance composites. Among these strategies, the use of buckypapers (BPs), thin films composed of three-dimensional networks of CNTs and/or GNP, has proven particularly effective. These thin films act as continuous porous structures that facilitate the infiltration of the polymer matrix while simultaneously preserving the electrical and mechanical connectivity of the nanocarbon network [12–14]. The combination of CNTs and GNPs within a single BP generates a synergistic effect: CNTs provide a flexible network of one-dimensional electrically conductive filaments, whereas GNPs contribute with high surface area, and two-dimensional conductivity, both nanomaterials exhibit excellent mechanical properties. This study aims [15]. Several studies investigated the preparation of hybrid BPs. Patole et al. [16] produced films containing 50 wt% CNTs and 50 wt% GNPs by wet filtration and compaction, using GNPs with thickness fewer than 10 layers and multi-walled carbon nanotubes (MWCNTs). The authors reported a 247% increase in electrical conductivity compared to BPs composed solely of CNTs. Dichiara et al. [17] also investigated the interaction between GNPs and CNTs in the formation of hybrid structures for adsorption applications, demonstrating that CNTs act as a three-dimensional conductive network into which GNPs are incorporated, thereby increasing the contact area and, consequently, the adsorption efficiency. In this context, vacuum-assisted resin impregnation has proven to be an effective technique for achieving complete resin infiltration in hybrid BPs, resulting in improved interfacial adhesion [14, 18]. The integration of hybrid BPs into epoxy systems therefore represents a promising approach for developing advanced composites with superior mechanical and functional properties, capable of meeting the growing demand for multifunctional structural materials.

Wang et al. [7] investigated epoxy resin composites reinforced with CNTs-based BPs consolidated via hot-press molding. The results demonstrated that the addition of 39 wt% of CNTs in the form of BPs led to a significant increase in the storage modulus of the epoxy matrix, with a rise of 492% compared to the neat resin. Rojas et al. [8] studied glass fiber/epoxy resin composites using three MWCTs-based BP. The incorporation of the BPs in the laminates did not result in improvements in elastic modulus according to dynamic mechanical analysis (DMA); however, a decrease in shear properties was observed in both compression shear and interlaminar shear strength tests. Lui and Shen [9] evaluated epoxy/carbon fiber composites reinforced with BP produced by compression molding. The application of BP is intended to enhance the interlaminar performance of the composites. Interlaminar fracture toughness tests revealed that the BP-reinforced composite exhibited superior behavior, with a critical strain energy release rate increase of up to 73%, raising the fracture load from 900 to 1000 N. In interlaminar shear strength (ILSS) tests, the BP-containing material also demonstrated a 29% improvement.

In this context, a fundamental question remains insufficiently explored: how the architecture and composition of hybrid MWCNT/GNP buckypapers govern the multifunctional behavior of epoxy composites, and how the interaction between nanocarbon networks and polymer infiltration affects the structure–property relationship.

Therefore, this study investigates the fabrication of epoxy composites reinforced with hybrid buckypapers composed of MWCNTs and two types of graphene-related materials, NG and GNP. The hybrid BPs were produced via vacuum filtration and subsequently impregnated with epoxy resin by vacuum infusion. This study aims to elucidate how nanocarbon architecture, filler ratio, and resin content influence electrical conductivity, electromagnetic shielding effectiveness, viscoelastic behavior, thermal stability, and heat transport. By correlating microstructural features, interfacial interactions, and multifunctional performance, this study provides design insights into hybrid buckypaper interlayers as tunable platforms for engineering multifunctional epoxy composites.

2 | Experimental

2.1 | Materials

The hybrid buckypapers (BPs) were prepared using NG (CheapTubes, USA; ~25 layers, 8–15 nm thick, ~104 μm lateral size, 99% purity), GNP (CheapTubes, USA; <4 layers, <4 nm thick, 1–2 μm lateral size, >99% purity), and MWCNTs (NC7000, Nanocyl S.A. Belgium); 1.5 μm length, 9.5 nm diameter, aspect ratio of 158 and 90% purity.

Triton X-100 (Dinâmica Química Contemporânea Ltda. (Brazil); CMC = 0.22–0.24 mmol L^{-1}, MW = 646.87 g mol^{-1}) was used as a surfactant for nanomaterial dispersion and was subsequently removed using acetone (99.63% purity).

An electrospun polyacrylonitrile (PAN) mat (Mn = 267,000 g mol^{-1}, Radici Group, Brazil) served as a sacrificial support for BP formation and was later dissolved and removed using N,N-dimethylformamide (DMF, 99.65%) and isopropyl alcohol (99.8%), both supplied by Dinâmica Química Contemporânea Ltda (Brazil).

For the production of the composites, a Castropox 4307 FLEX/1209 epoxy resin supplied by Castro Composites (Spain)

15480569, 0, Downloaded from https://4spepublications.onlinelibrary.wiley.com/doi/10.1002/pc.71490 by Braian Buitrago Uribe - Universidade Do Minho , Wiley Online Library on [06/08/2026]. See the Terms and Conditions (https://onlinelibrary.wiley.com/terms-and-conditions) on Wiley Online Library for rules of use; OA articles are governed by the applicable Creative Commons License

was used. The epoxy resin Castropox 4307 FLEXis produced by the condensation of bisphenol A-F and epichlorhydin, with an epoxy index of (0.52 ± 0.02) (100/192), viscosity of (700 ± 70) mPa s at 25°C, density of 1.13 g/cm^3 at 20°C, flash point of approximately 130°C, color index < 2, and an epoxy equivalent weight of 192 g/eq. The hardener (Castropox 1209) has an amine value of (325 ± 15) mg KOH/g, density of 1.03 g/cm^3 at 20°C, flash point of 130°C, viscosity (270 ± 50) mPa s at 25°C, color index < 3, solids content of 100%.

2.2 | Preparation of PAN Electrospun Nanofibers (PEN)

Polyacrylonitrile (PAN) electrospun nanofiber mats (PEN) were produced following the procedure described by Oliveira Junior et al. [19]. PAN (1.5 g) was dissolved in N,N-dimethylformamide (DMF, 13.5 mL) under magnetic stirring at 100°C for 1 h at 120 rpm, followed by ultrasonic mixing for 30 min to ensure complete homogenization. The resulting solution was loaded into a 20 mL syringe equipped with a 30 mm × 0.8 mm needle and electrospun under the following conditions: room temperature of (25 ± 5)°C, relative humidity of (55 ± 5)%, infusion rate of 1.5 mL h^{-1}, tip-to-collector distance of 80 mm, collector rotation speed of 1000 rpm, and applied voltage of 14 kV [19, 20].

2.3 | Preparation of Buckypapers (BPs)

Hybrid buckypapers (BPs) were fabricated following the procedure described by Rojas et al. [21]. Table 1 summarizes the compositions and nomenclature of the prepared samples. Mixtures of MWCNTs, NG, and GNP at different weight ratios (0/100, 25/75, 50/50, and 75/25 wt%) were dispersed in 200 mL of distilled water containing 2 g of Triton X-100. The dispersion was carried out using a probe-type sonicator (Sonics Vibra-Cell VCX750, 20 kHz, 750 W) for 40 min at 40% amplitude in pulsed mode (5 s on/3 s off), with the sample placed in an ice bath to maintain the temperature below 25°C. The resulting suspension was centrifuged at 4000 rpm for 30 min to remove undispersed agglomerates.

TABLE 1 | Composition, filler ratio, and nomenclature of the fabricated hybrid buckypapers (BPs) composed of multiwalled carbon nanotubes (MWCNTs), nanographite (NG), and graphene nanoplatelets (GNP).

Samples	MWCNT (wt%)	NG (wt%)	GNP (wt%)
BP-N100	100	—	—
BP-NG25/75	25	75	—
BP-NG50/50	50	50	—
BP-NG75/25	75	25	—
BP-NGP25/75	25	—	75
BP-NGP50/50	50	—	50
BP-NGP75/25	75	—	25

The supernatant was vacuum-filtered through a nylon membrane (45 mm diameter, 0.45 μm pore size) with a PEN mat (45 × 45 mm) placed on its surface. During filtration, acetone was applied to facilitate surfactant removal. The obtained BPs were dried at room temperature for 15 h and subsequently separated from the PEN mat by selective dissolution of PAN. Each BP/PEN composite was immersed in 25 mL of DMF at 60°C for 10 min, followed by 25 mL of isopropyl alcohol for another 10 min. The final BPs were dried again at room temperature for 15 h.

2.4 | Vacuum Infusion of BPs With Epoxy for Sample Preparation

The composites were prepared by vacuum-assisted resin impregnation using hybrid BP films composed of MWCNT and graphene-related materials (GRMs). A schematic representation of the hybrid buckypaper preparation and vacuum-assisted epoxy infiltration process is presented in Figure 1. The previously obtained BP discs were placed in a flat mold, covered with a sealed plastic film, and connected to a vacuum pump. The epoxy resin was then introduced into the system and forced to infiltrate the porous network of the BP films according to the procedure described by Uribe et al. [22]. After impregnation, the system was maintained under vacuum until complete saturation. The impregnated buckypapers were then cured at room temperature for 24 h, followed by a post-curing treatment at 60°C for 2 h, according to the resin manufacturer's recommendations. Table 2 summarizes the compositions and nomenclature of the manufactured composites, where C stands for composites, BP stands for buckypaper, NG and GNP denote the graphene-related materials used, N100 represents the buckypaper composed of 100 wt% MWCNTs, and Neat refers to the epoxy resin without BP.

2.5 | Characterization of BPs and Composites

2.5.1 | Impedance Spectroscopy (IS)

The volume resistivity of the BPs and composites was determined by measuring the characteristic *I–V* curves at room temperature using a Keithley SourceMeter Unit (SMU 2635B, Keithley Instruments Inc., Cleveland, OH, USA) (Figure 2). Measurements were performed in the voltage range of −10 to +10 V with 0.5 V increments. The buckypaper specimens had an average thickness of approximately 0.2 mm and a diameter of 50 mm, whereas the composite specimens had an average thickness of approximately 0.6 mm and the same diameter. The current and voltage data were recorded, and the resistivity was calculated considering the geometric factors of each sample. Volume electrical conductivity was statistically analyzed by analysis of variance (ANOVA), followed by Tukey–Kramer post hoc testing, with a significance level of $p < 0.05$.

2.5.2 | Electromagnetic Interference Shielding Effectiveness

The electromagnetic interference shielding (EMI) measurements of BPs and composites were performed following the

15480569, 0, Downloaded from https://4spepublications.onlinelibrary.wiley.com/doi/10.1002/pc.71490 by Braian Buitrago Uribe - Universidade Do Minho , Wiley Online Library on [06/08/2026]. See the Terms and Conditions (https://onlinelibrary.wiley.com/terms-and-conditions) on Wiley Online Library for rules of use; OA articles are governed by the applicable Creative Commons License

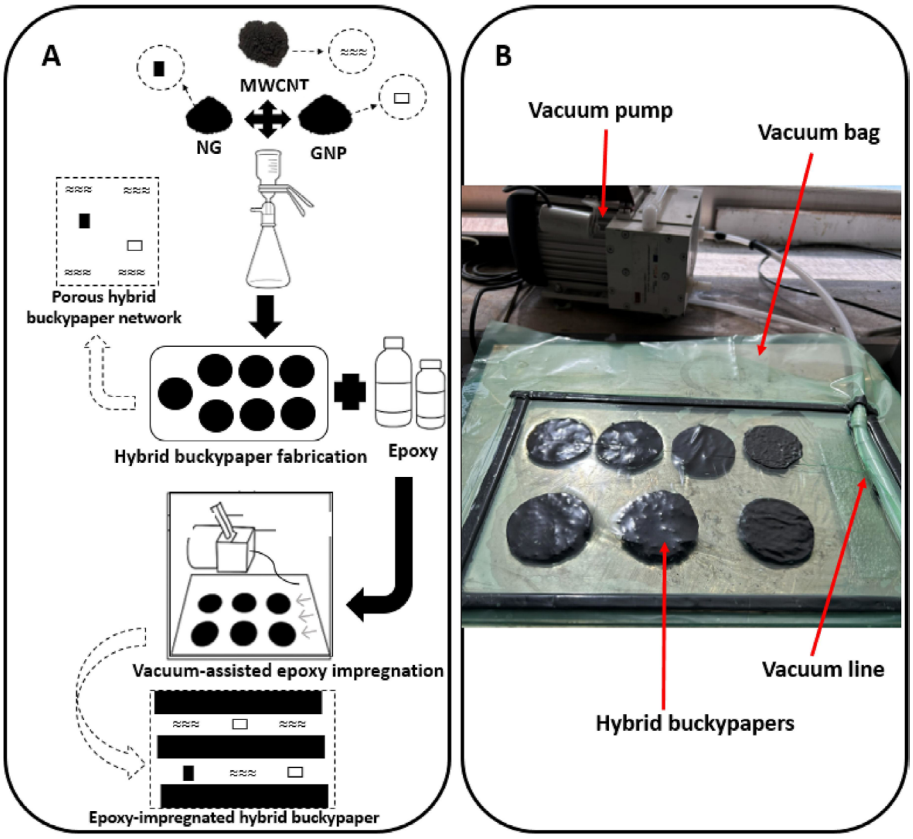


FIGURE 1 | (A) Schematic illustration of the fabrication of hybrid buckypapers composed of MWCNTs and graphene-related materials (nanographite or graphene nanoplatelets), followed by vacuum-assisted epoxy impregnation. Insets illustrate the porous conductive network before resin infiltration and the epoxy-filled hybrid network after impregnation. (B) Photograph of the vacuum-assisted epoxy impregnation setup used to fabricate the hybrid BP/epoxy composites.

TABLE 2 | Composition, filler ratio, and nomenclature of the epoxy composites reinforced with hybrid buckypapers.

Samples	BP-N100	BP-NG25/75	BP-NG50/50	BP-NG75/25	BP-GNP25/75	BP-GNP50/50	BP-GNP75/25
Neat							
C-N100	X						
C-NG25/75		X					
C-NG50/50			X				
C-NG75/25				X			
C-GNP25/75					X		
C-GNP50/50						X	
C-GNP75/25							X

Note: The table also summarizes the corresponding buckypaper designation used throughout the manuscript.

ASTM D4935-99 standard procedure [23]. Circular samples with a diameter of 60 mm were placed between two coaxial flanges maintaining a characteristic impedance of 50 Ω and connected to a Vector Network Analyzer (VNA, model R&SZVL3, Rohde & Schwarz, Munich, Germany) using two coaxial cables and two 10 dB 50 Ω attenuators. The shielding effectiveness (*SE*) was measured over the frequency range between 30 and 3000 MHz, corresponding to the radiofrequency spectrum typically used in automotive systems. According to ASTM D4935-99 standard, the method for measuring electromagnetic shielding effectiveness is considered normatively valid in the frequency range from 30 MHz to 1.5 GHz. This upper limit is associated with the physical limitations of the coaxial test system, specifically the practical cut-off frequency of the device. For frequencies above this range, the results were analyzed exclusively in a relative, comparative manner between samples, since all measurements were carried out using the same equipment, cables, system geometry, frequency range, and experimental procedure. According to ASTM D4935 standard, the shielding effectiveness (*SE*) is expressed as the ratio of the incident electric (*E*) or magnetic (*H*) field to the transmitted electric or magnetic field, as shown in Equation (1).

15480569, 0, Downloaded from https://4spepublications.onlinelibrary.wiley.com/doi/10.1002/pc.71490 by Braian Buitrago Uribe - Universidade Do Minho , Wiley Online Library on [06/08/2026]. See the Terms and Conditions (https://onlinelibrary.wiley.com/terms-and-conditions) on Wiley Online Library for rules of use; OA articles are governed by the applicable Creative Commons License

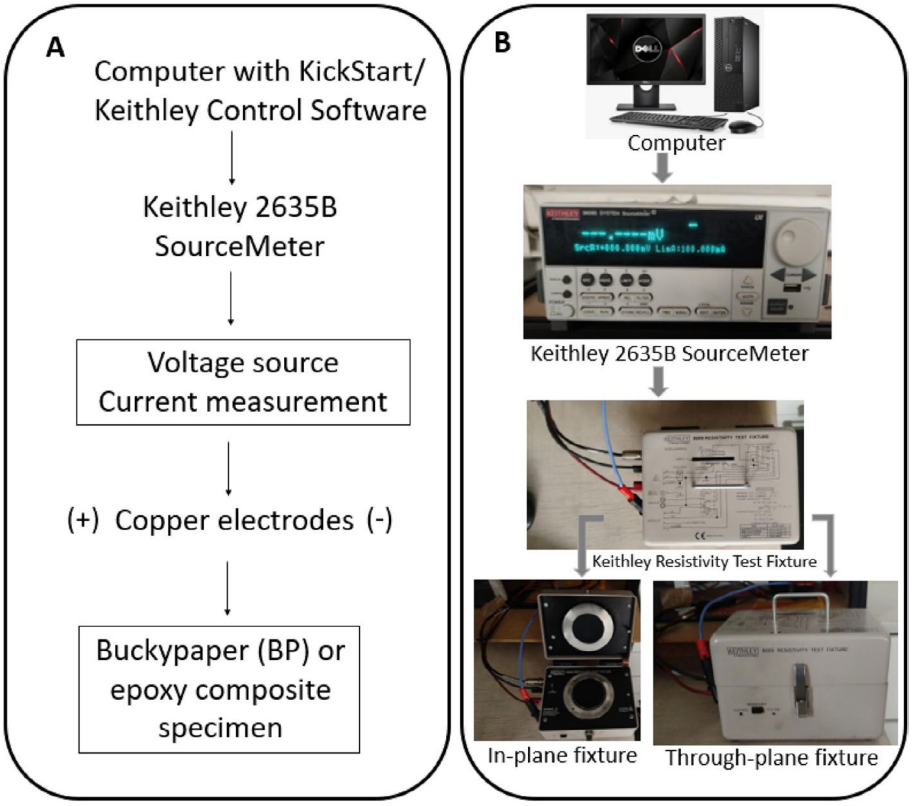


FIGURE 2 | Electrical conductivity measurement setup. (A) Schematic illustration of the experimental configuration used for electrical conductivity measurements. The Keithley 2635B SourceMeter was controlled by a computer and operated in source-voltage/measure-current mode. Copper electrodes were connected to the buckypaper or epoxy composite specimens. (B) Photographs of the experimental setup, including the computer, Keithley 2635B SourceMeter, Keithley resistivity test fixture, and the in-plane and through-plane measurement fixtures.

$$SE\,(\mathrm{dB}) = 20\log 10\left(\frac{E,H\ \text{incident}}{E,H\ \text{transmitted}}\right) \quad (1)$$

2.5.3 | Thermogravimetric Analysis

Thermogravimetric analysis (TGA) of the BPs and composites was conducted using a Netzsch Iris TG F1 instrument. Samples of ~0.01 g were heated from 40°C to 700°C at a rate of 20°C/min under nitrogen and synthetic air flow of 50 mL min^{-1}.

The epoxy resin content was estimated from the TGA residue using Equation (2). No independent gravimetric determination of the resin uptake was performed. The resin mass fraction in the composites was estimated from the TGA data. The residual mass fraction (*fr*) of each sample was determined as the remaining mass percentage after complete thermal decomposition of the organic components. Assuming additive contributions from each component to the final residue, the resin mass fraction (*fr*) in the composites was calculated using Equation (2).

$$fr = \frac{Rcomp - Rbp}{Rr - Rbp} \quad (2)$$

where *Rcomp*, *Rbp*, *Rr* are the residual mass fractions of the composite, the BP, and the neat resin, respectively.

This approach provides an estimate of the resin content impregnated into the BP, based on the relative residual masses of the individual components.

2.5.4 | DMA

DMA was performed according to ASTM D7028 using a TA Instruments Q800 dynamic mechanical analyzer operating in three-point bending mode. The tests were conducted at a heating rate of 2°C min^{-1}, a frequency of 1 Hz, over the temperature range from −20°C to 100°C, with an initial isothermal hold of 2 min. Rectangular specimens with average dimensions of approximately 36 mm × 9.7 mm × 4.8 mm (length × width × thickness) were tested. The glass transition temperature (Tg) was determined from the peak of the tan δ curve.

2.5.5 | Field-Emission Gun Scanning Electron Microscopy

Morphological characterization of composites was performed using a FEI NOVA 200 ultra-high-resolution scanning electron microscope (FEG/SEM) in secondary electron (SE) mode at a power of 10 kV. A thin layer of gold was applied to each surface to enhance the sample's conductivity.

2.5.6 | Thermal Conductivity (Through-Plane)

The through-plane thermal conductivity was determined using a laser flash apparatus (LFA 447 NanoFlash, Netzsch-Gerätebau GmbH, Selb, Germany). Measurements were performed at 25°C. Square specimens with dimensions of approximately

15480569, 0, Downloaded from https://4spepublications.onlinelibrary.wiley.com/doi/10.1002/pc.71490 by Braian Buitrago Uribe - Universidade Do Minho , Wiley Online Library on [06/08/2026]. See the Terms and Conditions (https://onlinelibrary.wiley.com/terms-and-conditions) on Wiley Online Library for rules of use; OA articles are governed by the applicable Creative Commons License

20 mm × 20 mm were used for the measurements. The thermal diffusivity was obtained from the time–temperature response, and the thermal conductivity was calculated using the measured density (buoyancy method) and the specific heat capacity determined by comparison with the Pyroceram 9606 reference material. The reported values correspond to the average of two measurements.

3 | Results and Discussion

3.1 | Electrical Conductivity

Figure 3 presents the electrical volumetric conductivity and resistivity results of the BPs and their corresponding epoxy composites. As expected, all freestanding BPs exhibited significantly higher conductivity than the composites, reflecting the presence of a continuous percolated carbon network prior to resin impregnation. In contrast, the incorporation of epoxy partially disrupted conductive pathways, reducing charge transport efficiency across the hybrid structure.

Among the BPs, the BP-N100 sample (100 wt% MWCNT) displayed the highest electrical conductivity (~9.24×10^{-3} S m^{-1}), which can be attributed to the formation of an interconnected nanotube network that promotes efficient charge transport. The incorporation of GRM (NG or GNP) led to a decrease in conductivity, likely due to partial disruption of MWCNT–MWCNT contacts.

However, hybrids containing GNP (BP-GNP25/75) exhibited improved electrical performance compared with NG-based counterparts, suggesting a more effective synergistic interaction between MWCNTs and the thinner, few-layer graphene sheets. In absolute terms, the conductivities observed for the BPs (in the range of 10^{-3} S m^{-1}) indicate a clearly conductive behavior, typical of percolated nanocarbon networks, although still far from metallic conduction. These values fall within the range commonly reported for hybrid BPs fabricated by vacuum filtration [12, 16, 20]. The composites exhibited cond0uctivities approximately two orders of magnitude lower, due to the insulating nature of the epoxy matrix, which disrupts the continuity of the conductive network. Nevertheless, the measured values remain within the range typical of conductive polymer composites (10^{-5} S m^{-1}), confirming that the internal structure of the BPs partially preserves its electrical connectivity after resin impregnation. These findings demonstrate that the electrical performance of the composites is primarily governed by the architecture and integrity of the embedded nanocarbon network, highlighting the critical role of dispersion quality, the MWCNT/GRM ratio, and the resin infiltration conditions.

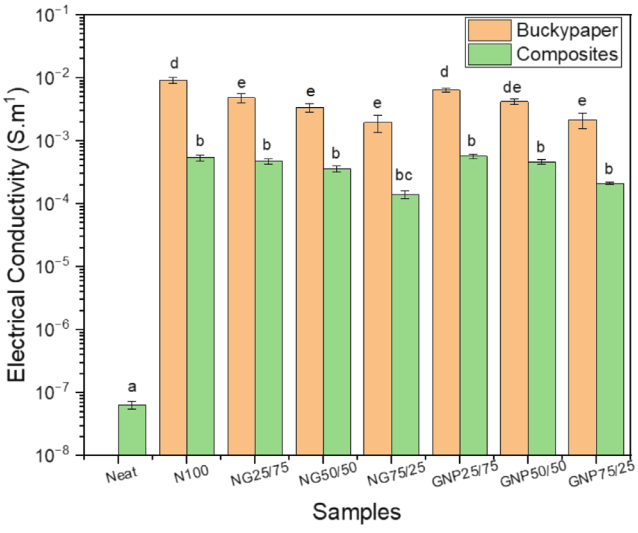


FIGURE 3 | Volume electrical conductivity of the fabricated hybrid buckypapers (orange bars) and the corresponding epoxy composites (green bars) measured at room temperature using the current–voltage (*I–V*) method. Mean values followed by the same letter do not differ by the Tukey–Kramer test at the 0.05 level of significance.

The higher electrical conductivity of the hybrid buckypapers containing GNPs is attributed to the formation of a more efficient conductive network. The large lateral dimensions and high aspect ratio of GNPs promote electron transport by increasing the contact area between adjacent carbon nanostructures and reducing junction resistance.

The composites cannot be classified as electrically conductive materials, however they exhibit charge-dissipative behavior, suitable for several sensing applications and for applications requiring electrostatic discharge control. The decrease in resistivity confirms effective impregnation of the conductive buckypaper network within the epoxy matrix, establishing electrical pathways across the hybrid structure [24, 25].

The electrical performance of the hybrid systems is therefore governed by three main factors: (i) continuity of the MWCNT network, (ii) morphology and thickness of graphene-related materials, and (iii) degree of resin infiltration within the porous buckypaper structure. Systems with lower resin content and effective nanocarbon interconnectivity exhibited higher conductivity, reinforcing the role of network integrity in determining multifunctional performance.

These findings indicate that hybrid buckypaper architecture acts as a tunable conductive framework within the epoxy matrix, where the balance between nanocarbon dispersion and polymer infiltration defines the final electrical response of the composites.

3.2 | Electromagnetic Shielding Effectiveness

Figure 4 presents the shielding effectiveness (SE) values as a function of frequency for the single phases (Figure 4A) and their corresponding composites (Figure 4B) in the 0–3000 MHz range of frequency. In Figure 4A, it is possible to observe that most samples exhibited positive SE values throughout the measured range, confirming their ability to attenuate electromagnetic radiation. For the neat resin, within the valid frequency range, the incident and transmitted fields were similar, indicating that the material cannot attenuate the energy through any dissipation mechanism, resulting in SE values close to zero.

The SE values were strongly dependent on the graphene-related material type and the MWCNT/GRM ratio. BP incorporating GNP exhibited superior performance, particularly BP-GNP25/75 which reached peak SE values around 60 dB at 800 MHz and

15480569, 0, Downloaded from https://4spepublications.onlinelibrary.wiley.com/doi/10.1002/pc.71490 by Braian Buitrago Uribe - Universidade Do Minho , Wiley Online Library on [06/08/2026]. See the Terms and Conditions (https://onlinelibrary.wiley.com/terms-and-conditions) on Wiley Online Library for rules of use; OA articles are governed by the applicable Creative Commons License

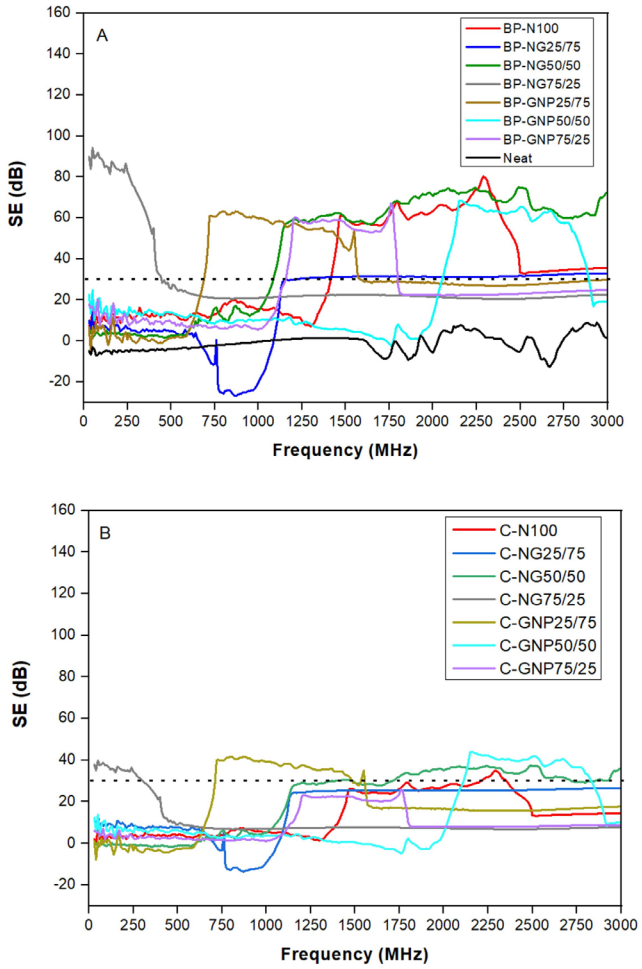


FIGURE 4 | Electromagnetic interference (EMI) shielding effectiveness as a function of frequency for (A) hybrid buckypapers and (B) hybrid BP/epoxy composites. The dashed horizontal line indicates the minimum shielding effectiveness generally considered suitable for practical EMI shielding applications.

BP-GNP50/50, which reached peak SE values around 65 dB at 2150 MHz. This enhancement can be attributed to the synergistic effect between the high aspect ratio of MWCNTs and the large surface area and intrinsic electrical conductivity of GNP, which promote the formation of a dense and interconnected conductive network. In contrast, the BPs containing NG showed less stable behavior with pronounced fluctuations, suggesting poorer dispersion or weaker interfacial contact between the nanofillers.

The BP-N100 sample, composed solely of MWCNTs, exhibited moderate SE values, indicating that the incorporation of GRM plays a key role in improving the shielding capability. High attenuation behavior in BPs has previously been reported by Ribeiro et al. [26, 27], and the synergistic interaction between MWCNTs and GRMs contributes to the improved electrical conductivity and, consequently, to the excellent shielding performance.

In Figure 4B, as expected, the overall SE values are lower than those of the freestanding BPs due to the insulating nature of the epoxy matrix, which partially disrupts the conductive pathways. Nevertheless, the trends observed for the BPs are maintained: composites containing BP-GNP25/75 and BP-GNP50/50 achieved the highest SE, reaching up to 40 dB in certain frequency ranges (at 730 and 2160 MHz). This finding demonstrates that the hybrid MWCNT/GRM structure remains effective even after integration into the composite laminate. For different applications, it is difficult to use BPs in their neat form due to issues related to the inherent fragility of the material, as well as the possibility of galvanic corrosion when carbonaceous elements come into contact with aluminum surfaces, which necessitates the development of an appropriate BP-based composite.

The improved SE can be ascribed to the multiple reflection and absorption processes arising from the well-connected conductive network within the BP and its interfacial contact with the epoxy matrix. These results confirm that the use of hybrid BPs, particularly those enriched with GNP, represents a highly effective strategy for enhancing the electromagnetic shielding performance of polymer matrix composites. Several studies indicate that the combination of CNTs and GNP creates a hybrid conductive network that favors both the reflection and absorption of electromagnetic radiation [28, 29], and this approach has been highlighted as promising in recent reviews on EMI shielding materials [30].

These results demonstrate that the synergy between MWCNTs and GRMs is essential for achieving high shielding efficiency, with the 25/75 ratio (MWCNT/GRM) being particularly favorable. The GNP-based hybrids maintain the efficient conductive pathways and enhance electromagnetic adsorption, even after incorporation of the epoxy matrix.

The electrical conductivity measurements of the BPs (Figure 3) show qualitative agreement with the shielding effectiveness (SE) results (Figure 4). BPs with the highest electrical conductivity (BP-GNP25/75) exhibit the highest SE values, demonstrating that a continuous conductive network promotes both electromagnetic reflection and absorption. The incorporation of these BPs into the epoxy matrix reduces the effective conductivity of the composites and, consequently, the overall SE. However, the performance hierarchy among the formulations is preserved, as composites containing the more conductive BPs maintain superior SE values.

The correlation between electrical conductivity and shielding effectiveness is evident: samples with higher conductivity exhibited superior SE values, confirming that network continuity plays a decisive role in electromagnetic attenuation. However, shielding performance is not governed solely by conductivity, but also by microstructural factors such as filler morphology, interfacial coupling, and dispersion quality, which influence wave propagation and energy dissipation within the composite.

The different performances observed for NG- and GNP-based systems can be attributed to their distinct morphological characteristics. GNP generally possess a higher aspect ratio, fewer stacked graphene layers, and a larger specific surface area than NG. These features promote more effective interfacial contact with MWCNTs, facilitating the formation of a continuous conductive network that enhances electron transport and, consequently, electrical conductivity and EMI shielding effectiveness. In contrast, NG consists of thicker graphitic particles with a

15480569, 0, Downloaded from https://4spepublications.onlinelibrary.wiley.com/doi/10.1002/pc.71490 by Braian Buitrago Uribe - Universidade Do Minho , Wiley Online Library on [06/08/2026]. See the Terms and Conditions (https://onlinelibrary.wiley.com/terms-and-conditions) on Wiley Online Library for rules of use; OA articles are governed by the applicable Creative Commons License

lower effective aspect ratio, which may reduce the number of conductive junctions within the hybrid network.

These results demonstrate that hybrid MWCNT/GRM buckypapers function as effective multifunctional interlayers, capable of imparting electromagnetic shielding ability to otherwise insulating epoxy systems while maintaining structural integrity. The 25/75 MWCNT/GRM ratio appears particularly favorable for balancing network connectivity and electromagnetic absorption efficiency, highlighting the importance of hybrid architecture in designing EMI-functional structural composites.

As discussed for the electrical conductivity results, the improved conductive network formed by GNPs directly contributes to the enhanced EMI shielding effectiveness. The higher electrical conductivity increases reflection losses, while the numerous conductive interfaces also favor multiple internal reflections and absorption of electromagnetic waves.

However, the mechanical response was not governed exclusively by the graphene-related material. Factors such as filler dispersion, resin infiltration into the buckypaper, and filler–matrix interfacial adhesion also contributed to the viscoelastic behavior of the composites. Consequently, the overall multifunctional performance resulted from the combined influence of filler morphology and composite microstructure rather than from the graphene-related material alone.

These observations are consistent with previous studies reporting that the synergistic combination of one-dimensional MWCNTs and two-dimensional GNP promotes more efficient conductive network formation than thicker graphitic particles, thereby improving the electrical performance of hybrid epoxy composites [31–33].

3.3 | Thermogravimetric Analysis

Figure 5 shows the TGA and the first derivative of the TGA (DTG) curves of the BPs and composites obtained under an inert atmosphere (nitrogen). The main thermal parameters, namely, the initial temperature ($T_{initial}$), the temperature at maximum degradation rate (T_{max}), the final temperature (T_{final}), residual mass at 700°C, and resin mass fraction (*fr*) in the composites,

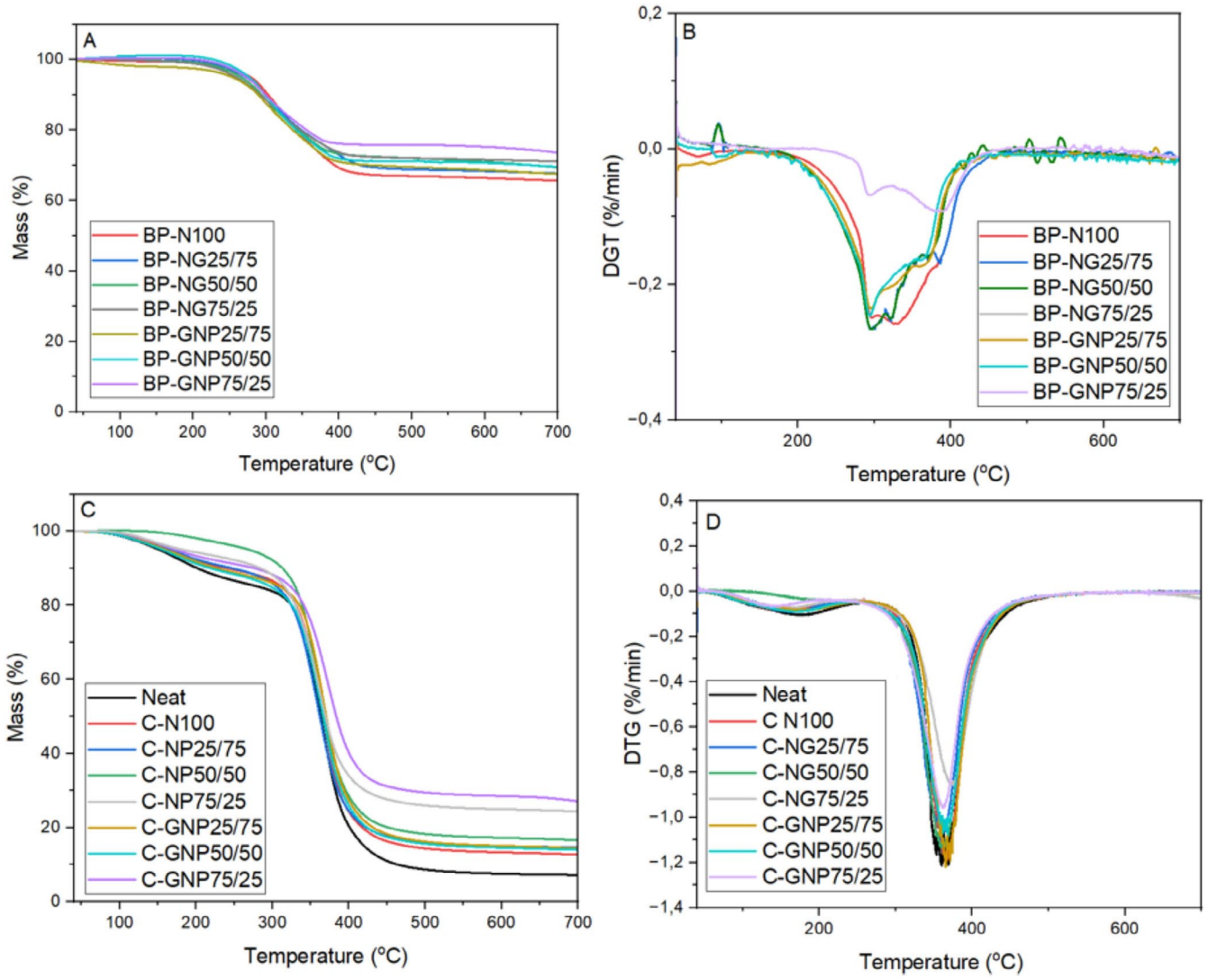


FIGURE 5 | Thermogravimetric analysis of the investigated materials: (A) TGA curves of the hybrid buckypapers, (B) corresponding derivative thermogravimetric (DTG) curves, (C) TGA curves of the hybrid BP/epoxy composites, and (D) corresponding DTG curves.

15480569, 0, Downloaded from https://4spepublications.onlinelibrary.wiley.com/doi/10.1002/pc.71490 by Braian Buitrago Uribe - Universidade Do Minho , Wiley Online Library on [06/08/2026]. See the Terms and Conditions (https://onlinelibrary.wiley.com/terms-and-conditions) on Wiley Online Library for rules of use; OA articles are governed by the applicable Creative Commons License

are summarized in Table 3. Therefore, the calculated resin contents should be considered approximate values and were used primarily for comparative analysis among the different composite systems. The initial degradation temperature ($T_{initial}$) was determined from the intersection of the baseline with the tangent drawn at the inflection point of the main weight-loss step. Due to the nature of carbon-based materials [34–37], both MWCNT and GRM react with oxygen at temperatures close to 300°C, leading to combustion. Therefore, these nanomaterials should only be used under oxidizing atmospheres at temperatures below 250°C to preserve their structural integrity [38, 39].

The BPs exhibited excellent thermal stability, with $T_{initial}$ values between 265°C and 267°C and T_{max} ranging from 294°C to 304°C. The residual mass at 700°C was remarkably high, between 65.7% and 73.8%, confirming the high carbon content and oxidation resistance of the MWCNT/GRM structures. Among the formulations, BP-GNP75/25 showed the highest residue (73.8%), indicating that a balanced combination of MWCNTs and GRM leads to a more thermally stable network, possibly due to the formation of a denser and more interconnected structure. The slight variations in T_{max} among the samples suggest that the MWCNT/GRM ratio marginally affects the initial degradation temperature but has a pronounced influence on the final residue, evidencing a synergistic effect between both carbon nanostructures.

The TGA curves of the composites (Figure 5C,D) exhibited a minor initial mass loss below ~200°C for all samples, which is attributed to the evaporation of absorbed moisture and residual low molecular weight compounds. The main thermal degradation step occurred above ~271°C–285°C, corresponding to the scission of the crosslinked epoxy structure. The neat epoxy (Neat) showed a maximum degradation rate (T_{max}) at 365°C and a residual mass of 7.1% at 700°C.

In contrast, the BP reinforced composites exhibited T_{max} values in the range of 256°C–373°C, depending on composition, together with significantly higher residual masses (12.5%–26.9%). The increased char yield is attributed to the presence of carbonaceous nanostructures within the buckypaper, which promote the formation of a thermally stable carbon rich residue during pyrolysis. Among the formulations, sample C-GNP75/25 presented the highest residual mass (26.9%), indicating enhanced resistance to thermal degradation and improved char forming capability. The improved thermal stability can be mainly attributed to the barrier effect of the buckypaper, which facilitates the formation of a protective carbonaceous layer and restricts heat and mass transfer during degradation, thereby slowing the diffusion of volatile decomposition products.

Overall, the incorporation of BP, particularly the hybrid MWCNT/GRM formulations, enhances the thermal stability and char formation of the composites. This behavior can be attributed to the intrinsic thermal stability of the nanocarbons and the formation of a three-dimensional interconnected network that hinders the propagation of thermal degradation. The variation in epoxy resin content (*fr*) directly influenced the electrical, electromagnetic shielding effectiveness, and dynamic-mechanical properties of the composites. Composites with lower resin fractions (C-GNP25/75) showed higher

TABLE 3 | Thermal degradation parameters obtained from thermogravimetric analysis (TGA) of the hybrid buckypapers and epoxy composites, including the onset degradation temperature ($T_{initial}$), temperature of maximum degradation rate (T_{max}), endset degradation temperature (T_{endset}), and residual mass at 700°C.

Samples	$T_{initial}$ (°C)	T_{max} (°C)	T_{endset} (°C)	Residual mass at 700°C (%)	*fr* (%)
BP-N100	266	296	438	65.7	—
BP-NG25/75	264	294	442	67.4	—
BP-NG50/50	263	298	443	69.5	—
BP-NG75/25	267	304	471	70.9	—
BP-GNP25/75	265	297	477	67.6	—
BP-GNP50/50	266	294	453	69.7	—
BP-GNP75/25	267	298	432	73.8	—
Neat	285	365	506	7.1	—
C-N100	273	368	517	12.5	96.4
C-NG25/75	271	356	506	14.8	95.3
C-NG50/50	273	361	550	16.8	90.3
C-NG75/25	279	373	506	24.5	87.6
C-GNP25/75	275	364	522	14.5	86.7
C-GNP50/50	277	363	527	14.2	93.9
C-GNP75/25	278	362	507	27.2	94.8

15480569, 0, Downloaded from https://4spepublications.onlinelibrary.wiley.com/doi/10.1002/pc.71490 by Braian Buitrago Uribe - Universidade Do Minho , Wiley Online Library on [06/08/2026]. See the Terms and Conditions (https://onlinelibrary.wiley.com/terms-and-conditions) on Wiley Online Library for rules of use; OA articles are governed by the applicable Creative Commons License

electrical conductivity and stronger electromagnetic shielding effectiveness responses, but inferior performance in the DMA analysis.

3.4 | DMA

Figure 6 presents the DMA curves depicting the temperature dependence of the storage modulus (E'), loss modulus (E''), and damping factor (tan δ) for the neat epoxy and the composites reinforced with hybrid buckypapers (BPs) composed of MWCNTs and graphene-related materials (GRMs). All samples exhibit the characteristic viscoelastic behavior of thermosetting polymers, with a high storage modulus in the glassy region, followed by a sharp decrease associated with the glass transition and a rubbery plateau at higher temperatures.

The main DMA parameters extracted from these curves are summarized in Table 4, including the glass transition temperature determined from the tan δ peak, the storage modulus (E') and loss modulus (E'') at 20°C, and the maximum tan δ values.

The neat epoxy exhibits a storage modulus of 1105 MPa at 20°C, along with a Tg of 46°C and the highest damping factor (tan $\delta_{max} = 0.60$), as shown in Table 5. The incorporation of hybrid BPs leads to a general reduction in stiffness, with E' (20°C) decreasing to values between 405 and 820 MPa depending on the composition. This behavior contrasts with many nanostructured epoxy systems reported in the literature [7, 40]. This reduction suggests that the presence of the preformed conductive network partially disrupts the continuity of the epoxy matrix, and that the wetting of the individual nanoparticles in the BP structure is not perfect, thus affecting stress transfer efficiency.

For NG-based composites (C-NG series), a clear dependence on composition is observed. The highest stiffness is obtained for C-NG50/50 (820 MPa), while further increasing the NG content

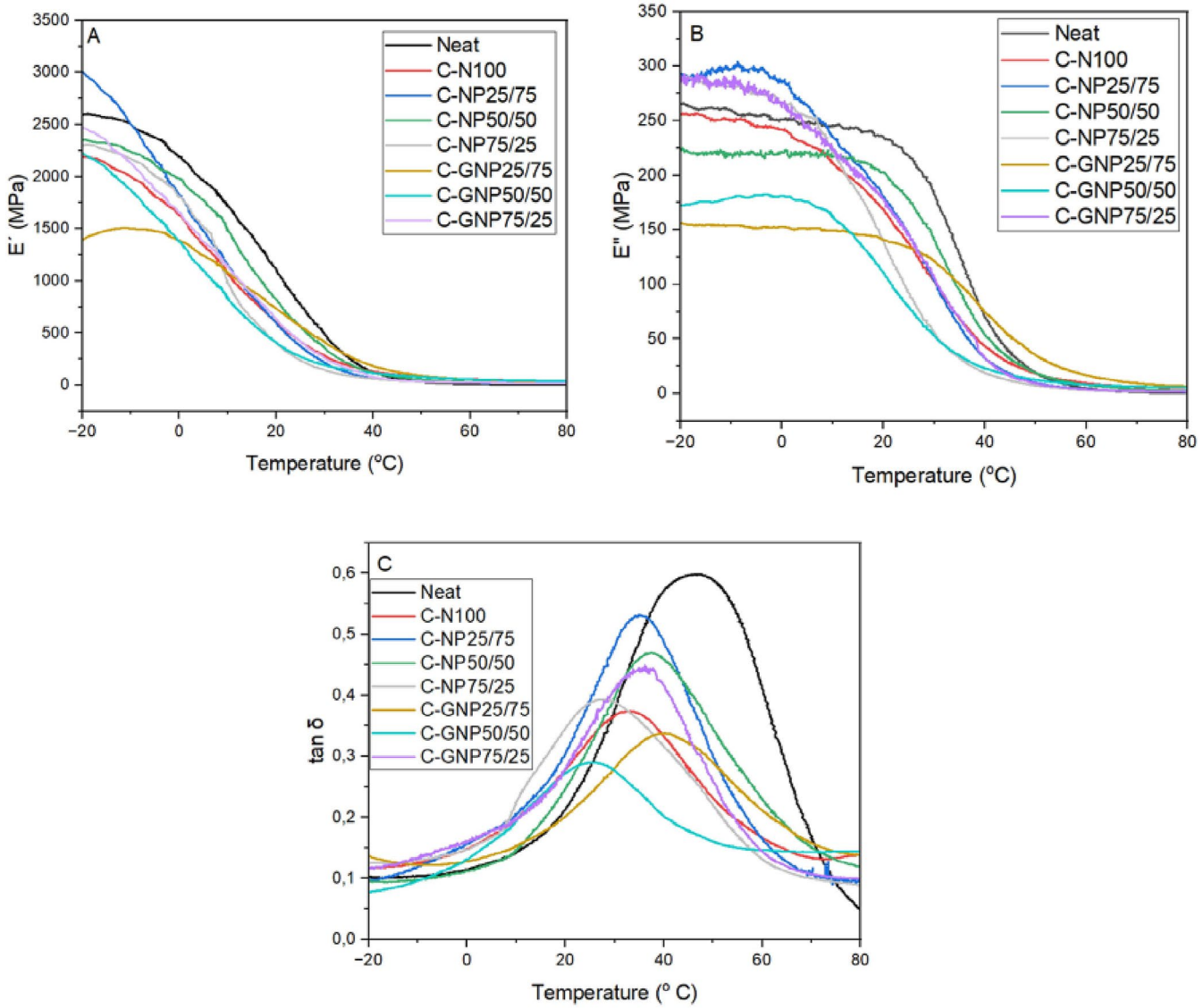


FIGURE 6 | Dynamic mechanical analysis (DMA) results of neat epoxy and hybrid BP/epoxy composites showing (A) storage modulus (E'), (B) loss modulus (E''), and (C) damping factor (tan δ) as a function of temperature. The glass transition temperature (Tg) was determined from the maximum of the tan δ peak.

15480569, 0, Downloaded from https://4spepublications.onlinelibrary.wiley.com/doi/10.1002/pc.71490 by Braian Buitrago Uribe - Universidade Do Minho , Wiley Online Library on [06/08/2026]. See the Terms and Conditions (https://onlinelibrary.wiley.com/terms-and-conditions) on Wiley Online Library for rules of use; OA articles are governed by the applicable Creative Commons License

TABLE 4 | Dynamic mechanical properties of neat epoxy and hybrid BP/epoxy composites obtained by dynamic mechanical analysis (DMA), including the glass transition temperature (Tg) determined from the tan δ peak, storage modulus (E'), loss modulus (E'') at 20°C, and maximum damping factor (tan δ_{max}).

Sample	T_g tan δ (°C)	E' (20) (MPa)	E'' (20) (MPa)	tan δ_{max} (–)
Neat	46	1105	234	0.60
C-N100	33	607	168	0.37
C-NG25/75	35	594	180	0.53
C-NG50/50	37	820	202	0.47
C-NG75/25	27	405	139	0.39
C-GNP25/75	40	699	141	0.34
C-GNP50/50	26	408	110	0.29
C-GNP75/25	36	637	178	0.45

TABLE 5 | Average density and through-plane thermal conductivity of the neat epoxy and hybrid BP/epoxy composites measured at room temperature.

Samples	Density mean value (g/cm^3)	Thermal conductivity (through-plane) (W/mK)
C-Neat	1.13	0.17 ± 0.03
C-N100	1.07	0.34 ± 0.11
C-NG25/75	1.05	0.28 ± 0.09
C-NG50/50	1.13	[a]
C-NG75/25	1.14	0.21 ± 0.06
C-GNP25/75	1.10	0.38 ± 0.13
C-GNP50/50	1.10	0.29 ± 0.06
C-GNP75/25	1.11	0.24 ± 0.02

[a]No measurement was possible because the laser passes through the sample having a very low thickness of 0.33 mm.

to 75/25 results in a significant decrease in E' to 405 MPa. This trend indicates that excessive NG content may impair wetting and interfacial adhesion, promoting structural heterogeneities, reducing the efficiency of load transfer within the composite. The loss modulus (E'') follows a similar tendency, decreasing from 202 (C-NG50/50) to 139 MPa (C-NG75/25), reinforcing the interpretation of reduced viscoelastic energy dissipation at higher NG contents.

In the case of GNP-based composites (C-GNP series), a different behavior is observed. The C-GNP25/75 formulation exhibits relatively high stiffness (699 MPa), while C-GNP50/50 shows a pronounced reduction in both E' (408 MPa) and E'' (110 MPa), indicating a less efficient stress transfer and lower energy dissipation capacity. Increasing the GNP proportion to 75/25 partially restores the mechanical response, with E' reaching 637 MPa and E'' increasing to 178 MPa. These results suggest that an optimal balance between MWCNTs and GNPs is required to achieve effective reinforcement, likely due to the combined effects of aspect ratio, dispersion, and interfacial interactions.

The glass transition temperatures determined from the tan δ peaks (Table 5) range from 26°C to 46°C. All composites exhibit Tg values lower than that of the neat epoxy, indicating increased chain mobility or a plasticization effect induced by the incorporation of BPs. The most pronounced reductions are observed for C-NG75/25 (27°C) and C-GNP50/50 (26°C), which also correspond to the lowest stiffness values, suggesting that these systems present less constrained polymer networks and weaker interfacial interactions. In contrast, composites such as C-GNP25/75 (40°C) and C-NG50/50 (37°C) retain relatively higher Tg values, indicating a greater restriction of segmental mobility due to more effective filler–matrix interactions.

The damping behavior, represented by tan δ_{max} (Table 5), further supports these observations. The neat epoxy shows the highest damping (0.60), while all composites exhibit lower values, ranging from 0.29 to 0.53. This reduction indicates restricted molecular mobility due to the presence of the conductive network. Among the composites, C-NG25/75 (0.53) shows relatively high damping, suggesting better energy dissipation capability, whereas C-GNP50/50 (0.29) presents the lowest value, indicating a more elastic and less dissipative response, possibly associated with structural heterogeneity and inefficient stress transfer.

Overall, the DMA results demonstrate that the incorporation of hybrid BPs significantly modifies the viscoelastic behavior of the epoxy matrix. A clear trade-off is observed between stiffness, glass transition temperature, and damping properties, which is strongly governed by the type of GRM and the MWCNT/GRM ratio. Compositions with more balanced filler ratios tend to exhibit improved mechanical performance when larger size GRM are mixed with MWCNT, while extreme compositions may lead to reduced stiffness and lower Tg due to poorer interfacial interactions and increased chain mobility.

The same interconnected carbon network responsible for the improved electrical conductivity also restricts the mobility of the epoxy chains, resulting in increased storage modulus and enhanced viscoelastic performance.

This interpretation is consistent with previous studies reporting that the synergistic interaction between MWCNTs and GNP improves stress transfer and constrains polymer chain mobility through the interconnected filler architecture, resulting in the observed viscoelastic behavior [31–33].

3.5 | Scanning Electron Microscopy

Figure 7 shows the FEG-SEM images of the cryo-fractured surfaces of the studied composites. The distinct morphologies of NG (red arrow) and GNP (orange arrow) are clearly distinguishable. As shown in Figure 7A, the epoxy/MWCNT BP composite (C-N100) exhibits a rough fracture surface, depicting efficient resin infiltration through the MWCNT network and good interfacial adhesion. Localized delamination can be observed in a few

15480569, 0, Downloaded from https://4spepublications.onlinelibrary.wiley.com/doi/10.1002/pc.71490 by Braian Buitrago Uribe - Universidade Do Minho , Wiley Online Library on [06/08/2026]. See the Terms and Conditions (https://onlinelibrary.wiley.com/terms-and-conditions) on Wiley Online Library for rules of use; OA articles are governed by the applicable Creative Commons License

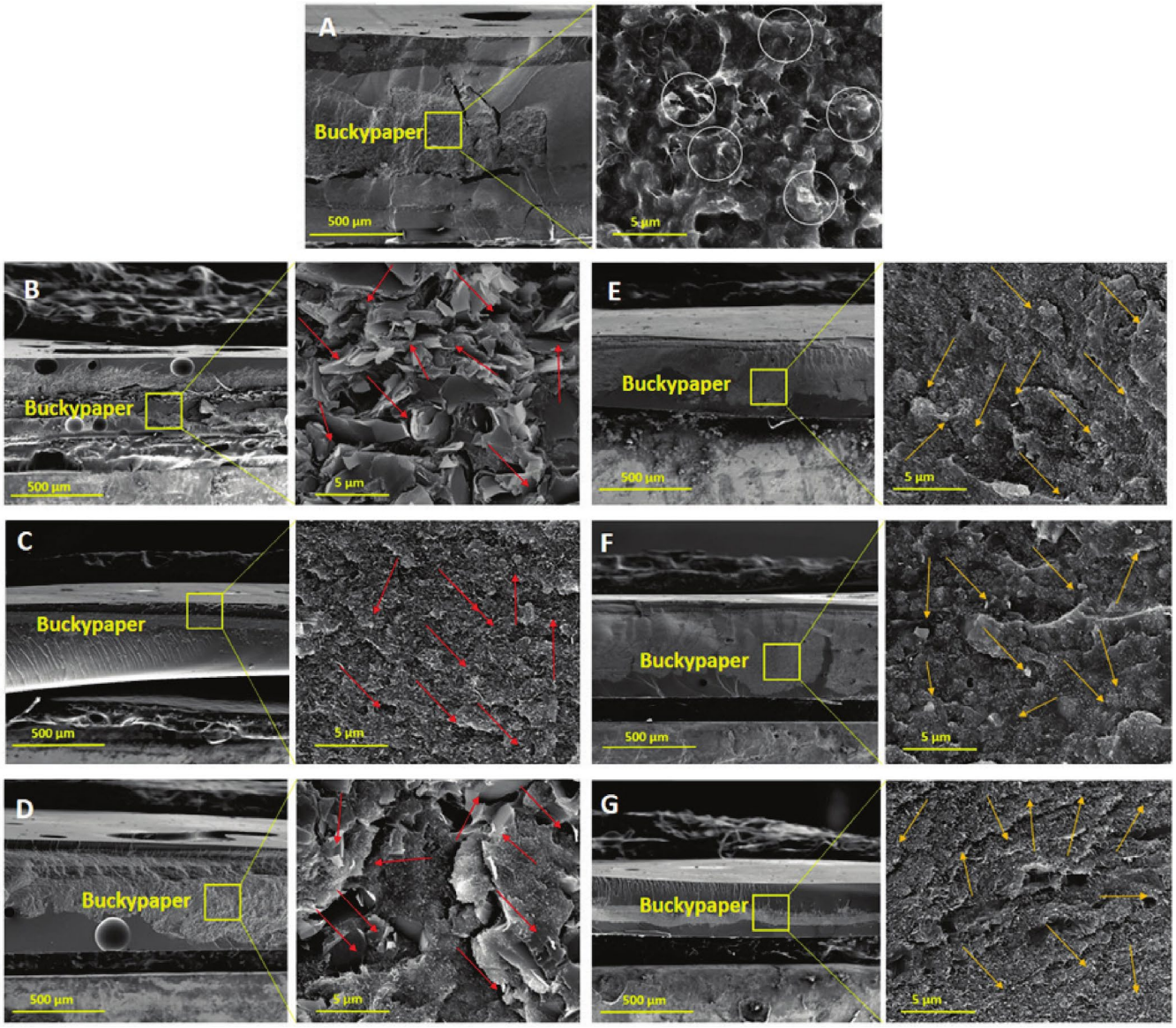


FIGURE 7 | Cross-sectional FEG-SEM micrographs of the epoxy composites reinforced with hybrid MWCNT/graphene-related material (GRM) buckypapers: (A) C-N100, (B) C-NG25/75, (C) C-NG50/50, (D) C-NG75/25, (E) C-GNP25/75, (F) C-GNP50/50, and (G) C-GNP75/25. Low-magnification images illustrate the overall laminate morphology and buckypaper distribution, whereas the corresponding high-magnification images highlight the microstructure of the conductive network, resin infiltration, and interfacial features between the hybrid buckypaper and the epoxy matrix.

spots on the borderline between the epoxy matrix and the BP. The presence of a network of CNTs (white circle in the magnified micrograph in Figure 7A), well wet by the matrix, was also observed, corroborating the efficiency of resin impregnation throughout the thickness of the BP.

FEG-SEM analysis confirms that the MWCNT/GRM ratio plays a decisive role in defining the interfacial morphology of the composites. For NG, Figure 7B (C-NG25/75) shows lamellar NG clusters, partial stacking of NG sheets, and the presence of voids that can weaken matrix-buckypaper cohesion. A more compact and homogeneous morphology is observed for the C-NG50/50 composite (Figure 7C), indicating efficient resin impregnation and a well-balanced interconnection between MWCNTs and NGs. Figure 7D (C-NG75/25) reveals a denser and more entangled structure, with fewer voids and well-bonded regions, indicating stronger interfacial adhesion and improved structural integrity.

For GNP-based composites, the C-GNP25/75 sample (Figure 7E) exhibits a smoother and denser surface, suggesting effective resin impregnation. The C-GNP50/50 composite (Figure 7F) exhibits a continuous and homogeneous surface without visible delamination, demonstrating a synergistic interaction between the MWCNTs and GNP that promotes optimized dispersion and strong interfacial adhesion. Finally, the C-GNP75/25 composite (Figure 7G) exhibits a compact and well-integrated interfacial structure, with evident resin penetration.

The predominance of GNP sheets combined with the three-dimensional MWCNTs network forms a continuous conductive architecture that enhances electron and phonon transport

15480569, 0, Downloaded from https://4spepublications.onlinelibrary.wiley.com/doi/10.1002/pc.71490 by Braian Buitrago Urbe - Universidade Do Minho , Wiley Online Library on [06/08/2026]. See the Terms and Conditions (https://onlinelibrary.wiley.com/terms-and-conditions) on Wiley Online Library for rules of use; OA articles are governed by the applicable Creative Commons License

throughout the composite. This microstructural arrangement explains the higher electrical conductivity and thermal stability, as MWCNTs act as conductive bridges between graphene layers, minimizing interfacial resistance and promoting efficient percolation. Overall, the microstructure observed for C-GNP75/25 confirms the synergistic interaction between MWCNTs and GNPs, resulting in a denser, more conductive, and thermally stable hybrid BP composite, consistent with its superior electrical, electromagnetic, and thermal performance.

Microstructural analysis by FEG-SEM, combined with TGA and DMA results, provides a coherent interpretation of the composite's behavior. FEG-SEM observations revealed that composites with lower resin content (C-GNP75/25) exhibited a more exposed and interconnected MWCNT/GNP network, whereas more impregnated composites (C-NG25/75) display MWCNTs and/NG more completely coated by the polymer matrix, which enhances interfacial adhesion. TGA results indicated that the less impregnated composites have higher residual masses, reflecting the greater relative contribution of the thermally stable buckypaper compared to the epoxy resin. This microstructure promotes the formation of a continuous conductive network, explaining the higher electrical and electromagnetic shielding performance. Conversely, the reduced resin fraction limits stress transfer and structural stiffness, as evidenced by the lower storage modulus in the DMA. Therefore, a clear trade-off is observed between electrical/electromagnetic performance and dynamic mechanical properties, primarily governed by the resin content in the composite.

3.6 | Thermal Conductivity (Through-Plane)

The through-plane thermal conductivity of epoxy-based composites was measured at 25°C, and the results are summarized in Table 5. All buckypaper-based composite systems exhibited higher thermal conductivity than the neat resin, confirming the contribution of the interconnected carbon nanomaterial network for heat transport. The MWCNT composite (C-N100) showed a through-plane thermal conductivity of approximately $0.34\,W\,m^{-1}\,K^{-1}$, associated with the formation of a continuous nanotube network facilitating phonon transport across the thickness.

The incorporation of graphene-related materials (GRMs) systematically modified the thermal transport behavior, depending on both GRM type and composition. For MWCNT/NG hybrids, thermal conductivity decreased with increasing NG content, reaching $0.21\,W\,m^{-1}\,K^{-1}$ for the C-NG75/25 composition. This behavior can be attributed to enhanced phonon scattering and increased interfacial thermal resistance associated with thicker or more defective graphene structures, which hinder efficient phonon coupling within the hybrid network. Similar interfacial effects have been reported in epoxy/CNT systems, where the encapsulation of CNTs by the polymer matrix significantly limits phonon transport across the composite thickness [41, 42].

In contrast, MWCNT/GNP-based buckypapers exhibited comparatively higher through-plane thermal conductivity, with the C-GNP25/75 composition reaching values up to $0.38\,W\,m^{-1}\,K^{-1}$. This enhancement reflects improved MWCNT–GNP interfacial contact and the formation of more efficient phonon transport pathways, promoted by the synergistic interaction between one-dimensional MWCNTs and thinner GNP. These results are consistent with recent findings on epoxy/SWCNT nanocomposites, where thermal transport was shown to be highly sensitive to filler morphology, dispersion quality, and interfacial resistance, leading to the existence of an optimal filler concentration for heat conduction [42].

The Neat resin exhibited the lowest thermal conductivity ($\approx 0.17\,W\,m^{-1}\,K^{-1}$), consistent with its intrinsically insulating and amorphous nature. Although the incorporation of hybrid buckypapers significantly enhances the through-plane thermal transport of the composite systems, the absolute values remain limited by interfacial thermal resistance and partial disruption of the conductive network by the polymer matrix, in agreement with previous reports on epoxy/CNT and epoxy/SWCNT composites.

For the C-NG50/50 composition, reliable through-plane thermal conductivity measurements could not be obtained due to excessive laser transmission through the thickness, possibly due to the presence of voids. This behavior indicates insufficient optical absorption and a lack of effective thermal continuity across the thickness, suggesting that an excessive NG content disrupts the percolated conductive network required for accurate thermal transport measurements.

Overall, these results demonstrate that through-plane thermal conductivity in CNT/GRM hybrid structures is not solely dictated by filler content, but rather by the combined effects of filler morphology, hybrid network architecture, and interfacial phonon scattering. When considered alongside electrical conductivity and EMI shielding effectiveness, a partial decoupling between phonon and electron transport is observed. MWCNT/GNP-based systems therefore exhibit a particularly favorable multifunctional balance, highlighting the potential of MWCNT/GRM hybrid buckypapers as multifunctional materials for applications requiring simultaneous electrical conduction, EMI shielding, and controlled thermal transport.

Although the interconnected carbon network favors electrical transport, the thermal conductivity is also strongly influenced by the quality of the filler-filler interfaces and phonon scattering, leading to a different trend from that observed for electrical conductivity.

4 | Conclusions

Hybrid buckypapers composed of MWCNTs and graphene-related materials (NG and GNP) were successfully fabricated and integrated into epoxy matrices, enabling the development of multifunctional composites through a controllable interlayer architecture. The results demonstrate that the multifunctional response of these systems is governed primarily by the continuity of the nanocarbon network, the morphology of the graphene-related materials, and the degree of resin infiltration within the buckypaper structure.

15480569, 0, Downloaded from https://4spepublications.onlinelibrary.wiley.com/doi/10.1002/pc.71490 by Braian Buitrago Uribe - Universidade Do Minho , Wiley Online Library on [06/08/2026]. See the Terms and Conditions (https://onlinelibrary.wiley.com/terms-and-conditions) on Wiley Online Library for rules of use; OA articles are governed by the applicable Creative Commons License

A clear structure–property relationship was identified: formulations with higher network connectivity exhibited superior electrical conductivity and electromagnetic shielding effectiveness, while systems with greater resin impregnation and improved interfacial adhesion showed enhanced mechanical stability. This establishes a trade-off between electrical/electromagnetic performance and viscoelastic stiffness, highlighting the critical role of hybrid architecture and resin fraction in tailoring composite behavior.

Overall, the incorporation of graphene-related materials into the hybrid buckypapers significantly influenced the multifunctional performance of the composites. GNP-containing systems generally exhibited higher electrical conductivity and EMI shielding effectiveness due to the formation of more efficient conductive networks. However, the mechanical behavior was governed by the combined effects of filler morphology, composition, conductive network architecture, resin infiltration, and filler–matrix interactions, highlighting the complex balance required to optimize both functional and structural properties. Thermal analyses confirmed that hybrid buckypapers act as thermally stable conductive frameworks within the epoxy matrix, while microstructural observations revealed that the interaction between nanocarbon morphology and polymer infiltration directly controls network integrity and multifunctional response.

Overall, hybrid MWCNT/GRM buckypapers function as tunable multifunctional interlayers, enabling the design of epoxy composites with tailored combinations of electrical conductivity, electromagnetic shielding, thermal stability, and mechanical performance. The results provide practical design guidelines for balancing structural and functional properties through control of filler architecture and resin content.

These findings position hybrid buckypaper-reinforced systems as promising candidates for lightweight structural materials requiring integrated electromagnetic management, electrostatic dissipation, and thermal functionality, particularly in aerospace, transportation, and electronic applications. This work demonstrates that hybrid buckypaper interlayers are not merely reinforcing elements, but active multifunctional design platforms capable of bridging structural and functional performance in polymer composites.

From an industrial perspective, vacuum-assisted resin impregnation is a scalable process widely employed in composite manufacturing. Nevertheless, the production cost of hybrid buckypapers remains one of the main challenges for large-scale implementation, primarily due to the cost of carbon nanomaterials and the need for controlled processing conditions. Continued advances in the production of graphene-related materials and optimization of buckypaper fabrication are expected to improve the economic feasibility of this technology.

Author Contributions

Rui Alexandre Araújo Ribeiro: methodology, formal analysis, writing – review and editing. **Rieyssa Maria de Almeida Corrêa:** writing – original draft, methodology, writing – review and editing. **Edson Cocchieri Botelho:** supervision, data curation, resources, writing – review and editing, visualization, validation, investigation, conceptualization. **Fabio Roberto Passador:** supervision, resources, formal analysis, validation, writing – review and editing, conceptualization. **Braian Esneider Buitrago Uribe:** investigation, methodology, validation, writing – review and editing, resources, supervision. **Michelle Leali Costa:** supervision, resources, writing – review and editing, validation, funding acquisition. **Maria Conceição Paiva:** funding acquisition, validation, supervision, resources, writing – review and editing, data curation, conceptualization. **Delfim Fernandes Soares:** methodology, writing – review and editing, supervision. **Thiély Ferreira da Silva:** writing – original draft, writing – review and editing, methodology, formal analysis. **Thais Ferreira da Silva:** conceptualization, investigation, funding acquisition, writing – original draft, methodology, writing – review and editing, visualization, formal analysis, software, project administration. **Beate Krause:** methodology, writing – review and editing, supervision.

Acknowledgments

The authors are grateful to grants: #2023/08407-4, 2024/11092-8, and 2024/11035-4, São Paulo Research Foundation (FAPESP) and CNPq (Conselho Nacional de Desenvolvimento Científico e Tecnológico), processes 306576/2020-1, 404875/2023-8, 305357/2023-9, 304964/2024-7 and 307933/2021-0. This study was financed in part by the Coordenação de Aperfeiçoamento de Pessoal de Nível Superior—Brasil (CAPES) - Finance Code 001. Authors also acknowledge the Fundação para a Ciência e Tecnologia—FCT with funding through the National Funds Reference, grant number UID/05256/2025 Institute for Polymers and Composites, University of Minho. The Article Processing Charge for the publication of this research was funded by the Coordenação de Aperfeiçoamento de Pessoal de Nível Superior - Brasil (CAPES) (ROR identifier: 00x0ma614).

Funding

This work was supported by Fundação de Amparo à Pesquisa do Estado de São Paulo (2023/08407-4, 2024/11092-8, 2024/11035-4), Conselho Nacional de Desenvolvimento Científico e Tecnológico (306576/2020-1, 404875/2023-8, 305357/2023-9, 304964/2024-7, 307933/2021-0), Coordenação de Aperfeiçoamento de Pessoal de Nível Superior (001), Fundação para a Ciência e Tecnologia—FCT (UID/05256/2025).

Conflicts of Interest

The authors declare no conflicts of interest.

Data Availability Statement

The data that support the findings of this study are available from the corresponding author upon reasonable request.

References

1. M. L. Costa, E. C. Botelho, and M. C. Rezende, "Monitoring of Cure Kinetic Prepreg and Cure Cycle Modeling," *Journal of Materials Science* 41, no. 13 (2006): 4349–4356, https://doi.org/10.1007/s10853-006-6082-1.

2. E. C. Botelho, N. Scherbakoff, and M. C. Rezende, "Porosity Control in Glassy Carbon by Rheological Study of the Furfuryl Resin," *Carbon* 39, no. 1 (2001): 45–52, https://doi.org/10.1016/S0008-6223(00)00080-4.

3. E. C. Botelho, C. L. Nogueira, and M. C. Rezende, "Monitoring of Nylon 6,6/Carbon Fiber Composites Processing by X-Ray Diffraction and Thermal Analysis," *Journal of Applied Polymer Science* 86, no. 12 (2002): 3114–3119, https://doi.org/10.1002/app.11335.

4. M. S. Dresselhaus, G. Dresselhaus, J. C. Charlier, and E. Hernández, "Electronic, Thermal and Mechanical Properties of Carbon Nanotubes," *Philosophical Transactions of the Royal Society A:*

15480569, 0, Downloaded from https://4spepublications.onlinelibrary.wiley.com/doi/10.1002/pc.71490 by Braian Buitrago Uribe - Universidade Do Minho , Wiley Online Library on [06/08/2026]. See the Terms and Conditions (https://onlinelibrary.wiley.com/terms-and-conditions) on Wiley Online Library for rules of use; OA articles are governed by the applicable Creative Commons License

Mathematical, Physical and Engineering Sciences 362, no. 1823 (2004): 2065–2098.

5. K. S. Novoselov, A. K. Geim, S. V. Morozov, et al., "Electric Field Effect in Atomically Thin Carbon Films," *Science* 306, no. 5696 (2004): 666–669, https://doi.org/10.1126/science.1102896.

6. H. Kim, A. A. Abdala, and C. W. Macosko, "Graphene/Polymer Nanocomposites," *Macromolecules* 43, no. 16 (2010): 6515–6530, https://doi.org/10.1021/ma100572e.

7. Z. Wang, Z. Liang, B. Wang, C. Zhang, and L. Kramer, "Processing and Property Investigation of Single-Walled Carbon Nanotube (SWNT) Buckypaper/Epoxy Resin Matrix Nanocomposites," *Composites Part A: Applied Science and Manufacturing* 35, no. 10 (2004): 1225–1232.

8. J. A. Rojas, L. A. Ardila-Rodríguez, M. F. Diniz, M. Gonçalves, B. Ribeiro, and M. C. Rezende, "Morphological, Mechanical, and Electromagnetic Interference Shielding Effectiveness Characteristics of Glass Fiber/Epoxy Resin/MWCNT Buckypaper Composites," *Journal of Applied Polymer Science* 138, no. 25 (2021): 50589.

9. L. Liu and L. L. Shen, "Influence of CNT Buckypaper on the Interlaminar Shear Strength of Laminates," in *Proceedings of the ICCM International Conference on Composite Materials* (Aalborg University, 2015), July 7–19.

10. Z. Spitalsky, D. Tasis, K. Papagelis, and C. Galiotis, "Carbon Nanotube–Polymer Composites: Chemistry, Processing, Mechanical and Electrical Properties," *Progress in Polymer Science* 35, no. 3 (2010): 357–401, https://doi.org/10.1016/j.progpolymsci.2009.09.003.

11. T. Kuilla, S. Bhadra, D. Yao, N. H. Kim, S. Bose, and J. H. Lee, "Recent Advances in Graphene Based Polymer Composites," *Progress in Polymer Science* 35, no. 11 (2010): 1350–1375, https://doi.org/10.1016/j.progpolymsci.2010.07.005.

12. A. Allaoui, S. Bai, H. M. Cheng, and J. B. Bai, "Mechanical and Electrical Properties of a MWNT/Epoxy Composite," *Composites Science and Technology* 62, no. 15 (2002): 1993–1998, https://doi.org/10.1016/S0266-3538(02)00129-X.

13. C. A. Martin, J. K. W. Sandler, M. S. P. Shaffer, et al., "Formation of Percolating Networks in Multi-Wall Carbon-Nanotube–Epoxy Composites," *Composites Science and Technology* 64, no. 15 (2004): 2309–2316, https://doi.org/10.1016/j.compscitech.2004.01.025.

14. Q. Li, C. Liu, Y. Wang, and S. Fan, "Superstrong and Stiff Carbon-Nanotube Films," *Advanced Materials* 19, no. 20 (2007): 3358–3363, https://doi.org/10.1002/adma.200602966.

15. M. F. De Volder, S. H. Tawfick, R. H. Baughman, and A. J. Hart, "Carbon Nanotubes: Present and Future Commercial Applications," *Science* 339, no. 6119 (2013): 535–539, https://doi.org/10.1126/science.1222453.

16. S. P. Patole, M. F. Arif, R. A. Susantyoko, S. Almheiri, and S. Kumar, "A Wet-Filtration-Zipping Approach for Fabricating Highly Electroconductive and Auxetic Graphene/Carbon Nanotube Hybrid Buckypaper," *Scientific Reports* 8 (2018): 12188, https://doi.org/10.1038/s41598-018-30009-4.

17. A. B. Dichiara, T. J. Sherwood, J. Benton-Smith, J. C. Wilson, S. J. Weinstein, and R. E. Rogers, "Free-Standing Carbon Nanotube/Graphene Hybrid Papers as Next Generation Adsorbents," *Nanoscale* 6 (2014): 6322–6327, https://doi.org/10.1039/C4NR01028K.

18. K. Jiang, Q. Li, and S. Fan, "Nanotechnology: Spinning Continuous Carbon Nanotube Yarns," *Nature* 419, no. 6909 (2002): 801, https://doi.org/10.1038/419801a.

19. M. S. Oliveira Junior, B. V. Manzolli Rodrigues, J. S. Marcuzzo, L. M. Guerrini, M. R. Baldan, and M. C. Rezende, "A Statistical Approach to Evaluate the Oxidative Process of Electrospun Polyacrylonitrile Ultrathin Fibers," *Journal of Applied Polymer Science* 134 (2017): 45458, https://doi.org/10.1002/app.45458.

20. J. A. Rojas, B. Ribeiro, and M. C. Rezende, "Influence of Serrated Edge and Rectangular Strips of MWCNT Buckypaper on the Electromagnetic Properties of Glass Fiber/Epoxy Resin Composites," *Carbon* 160 (2020): 317–327, https://doi.org/10.1016/j.carbon.2020.01.036.

21. J. A. Rojas, L. A. Ardila-Rodríguez, M. F. Diniz, M. Gonçalves, B. Ribeiro, and M. C. Rezende, "Optimization of Triton X-100 Removal and Ultrasound Probe Parameters in the Preparation of Multiwalled Carbon Nanotube Buckypaper," *Materials & Design* 166 (2019): 107612, https://doi.org/10.1016/j.matdes.2019.107612.

22. B. E. Uribe, A. C. Soares-Pozzi, and J. R. Tarpani, "Nanocellulose-Coated Carbon Fibers Towards Developing Hierarchical Polymer Matrix Composites," *Materials Today: Proceedings* 8 (2019): 820–831, https://doi.org/10.1016/j.matpr.2019.02.024.

23. ASTM D4935-99, "Standard Test Method for Measuring the Electromagnetic Shielding Effectiveness of Planar Materials," 1999.

24. T. F. D. Silva, F. Menezes, L. S. Montagna, A. P. Lemes, and F. R. Passador, "Preparation and Characterization of Antistatic Packaging for Electronic Components Based on Poly (Lactic Acid)/Carbon Black Composites," *Journal of Applied Polymer Science* 136, no. 13 (2019): 47273.

25. T. F. da Silva, F. Menezes, L. S. Montagna, A. P. Lemes, and F. R. Passador, "Synergistic Effect of Adding Lignin and Carbon Black in Poly (Lactic Acid)," *Polímeros* 30, no. 1 (2020): e2020002.

26. B. Ribeiro, J. A. R. Corredor, L. F. de Paula Santos, N. A. S. Gomes, and M. C. Rezende, "Electrical Conductivity and Electromagnetic Shielding Performance of Glass Fiber-Reinforced Epoxy Composites With Multiwalled Carbon Nanotube Buckypaper Interlayer," *Journal of Materials Science: Materials in Electronics* 32 (2021): 1962–1976.

27. B. Ribeiro, N. A. S. Gomes, and M. C. Rezende, "Lightweight Multi-Walled Carbon Nanotube Buckypaper/Glass Fiber–Epoxy Composites for Strong Electromagnetic Interference Shielding and Efficient Microwave Absorption," *Journal of Materials Science: Materials in Electronics* 32, no. 11 (2021): 14494–14508.

28. C.-L. Lin, J.-W. Li, Y.-F. Chen, J.-X. Chen, C.-C. Cheng, and C.-W. Chiu, "Graphene Nanoplatelet/Multiwalled Carbon Nanotube/Polypyrrole Hybrid Fillers in Polyurethane Nanohybrids With 3D Conductive Networks for EMI Shielding," *ACS Omega* 7, no. 49 (2022): 45697–45707, https://doi.org/10.1021/acsomega.2c06613.

29. N. Bagotia, V. Choudhary, and D. K. Sharma, "Synergistic Effect of Graphene/Multiwalled Carbon Nanotube Hybrid Fillers on Mechanical, Electrical and EMI Shielding Properties of Polycarbonate/Ethylene Methyl Acrylate Nanocomposites," *Composites Part B: Engineering* 159 (2019): 378–388, https://doi.org/10.1016/j.compositesb.2018.10.009.

30. M. S. Hareesh, P. Joseph, and S. George, "Electromagnetic Interference Shielding: A Comprehensive Review of Materials, Mechanisms, and Applications," *Nanoscale Advances* 7 (2025): 4510–4534, https://doi.org/10.1039/D5NA00240K.

31. B. M. Madhu, A. Rashmi, R. R. N. Sailaja, and J. Sundara Rajan, "Combined Effect of Multiwalled Carbon Nanotubes, Graphene Nanoplatelets, and Aluminum Trihydride on the Thermal Stability of Epoxy Composites," *Polymer Composites* 43, no. 3 (2022): 1343–1356, https://doi.org/10.1002/pc.26452.

32. B. M. Madhu and R. Aradhya, "Enhancement of Electrical Conductivity and Band Gap of Epoxy/MWCNT/GNP/Glass Fibers Hybrid Materials," *Journal of Adhesion Science and Technology* 39, no. 1 (2025): 1–16, https://doi.org/10.1080/01694243.2024.2390145.

33. B. M. Madhu, R. Aradhya, and J. Sundara Rajan, "Hydrothermal Aging of Glass Fiber Epoxy-Carbon Nanocomposites and Its Service Life Predictions Based on Tensile Strength," *Journal of Vinyl and Additive Technology* 30, no. 3 (2024): 772–787, https://doi.org/10.1002/vnl.22084.

34. K. Mitsuda, H. Kimura, and T. Murahashi, "Evaporation and Decomposition of Triton X-100 Under Various Gases and Temperatures,"

15480569, 0, Downloaded from https://4spepublications.onlinelibrary.wiley.com/doi/10.1002/pc.71490 by Braian Buitrago Uribe - Universidade Do Minho , Wiley Online Library on [06/08/2026]. See the Terms and Conditions (https://onlinelibrary.wiley.com/terms-and-conditions) on Wiley Online Library for rules of use; OA articles are governed by the applicable Creative Commons License

Journal of Materials Science 24 (1989): 413–419, https://doi.org/10.1007/BF01107420.

35. H. Marsh, I. A. S. Edwards, R. Menendez, et al., *Introduction to Carbon Science* (Butterworth-Heinemann, 1989).

36. G. R. Devi and K. R. Rao, "Carbon–Carbon Composites: An Overview," *Defence Science Journal* 43 (2013): 369–383, https://doi.org/10.14429/dsj.43.4085.

37. E. Savage, *Carbon–Carbon Composites* (Springer, 1993).

38. Z. P. Wu and J. N. Wang, "Preparation of Large-Area Double-Walled Carbon Nanotube Films and Application as Film Heater," *Physica E: Low-Dimensional Systems and Nanostructures* 42 (2009): 77–81, https://doi.org/10.1016/j.physe.2009.09.002.

39. P. M. Ajayan and S. Iijima, "Capillarity-Induced Filling of Carbon Nanotubes," *Nature* 361 (1993): 333–334, https://doi.org/10.1038/361333a0.

40. S. Sharma, B. P. Singh, S. S. Chauhan, et al., "Enhanced Thermomechanical and Electrical Properties of Multiwalled Carbon Nanotube Paper Reinforced Epoxy Laminar Composites," *Composites Part A: Applied Science and Manufacturing* 104 (2018): 129–138.

41. B. Krause, C. Barbier, J. Levente, M. Klaus, and P. Pötschke, "Screening of Different Carbon Nanotubes in Melt-Mixed Polymer Composites With Different Polymer Matrices for Their Thermoelectrical Properties," *Journal of Composites Science* 3, no. 4 (2019): 106, https://doi.org/10.3390/jcs3040106.

42. I. I. Patunrengi, S. Abdullahi, M. Aljaghtham, A. Alshahrie, and N. Salah, "Thermoelectric and Power Generation Properties of Epoxy/SWCNT Nanocomposite Above and Below Room Temperature," *Journal of Materials Science: Materials in Electronics* 36, no. 20 (2025): 1230, https://doi.org/10.1007/s10854-025-15351-4.

15480569, 0, Downloaded from https://4spepublications.onlinelibrary.wiley.com/doi/10.1002/pc.71490 by Braian Buitrago Uribe - Universidade Do Minho , Wiley Online Library on [06/08/2026]. See the Terms and Conditions (https://onlinelibrary.wiley.com/terms-and-conditions) on Wiley Online Library for rules of use; OA articles are governed by the applicable Creative Commons License